SpoIVA-SipL complex formation is essential for *Clostridioides difficile* spore assembly

Megan H. Touchette,[1]* Hector Benito de la Puebla,[1] Priyanka Ravichandran,[2] Aimee Shen[1,2#]

[1]Department of Molecular Biology and Microbiology, Tufts University School of Medicine, Boston, Massachusetts, USA, [2]Department of Microbiology and Molecular Genetics, University of Vermont, Burlington, Vermont, USA.

* Current address: Nova Biomedical, Waltham, MA, USA.

#Address correspondence to

Phone number: (802)656-9531

Aimee Shen, aimee.shen@tufts.edu

Phone number: (617)636-3792

Abstract

Spores are the major infectious particle of the Gram-positive nosocomial pathogen, *Clostridioides* (formerly *Clostridium*) *difficile*, but the molecular details of how this organism forms these metabolically dormant cells remain poorly characterized. The composition of the spore coat in *C. difficile* differs markedly from that defined in the well-studied organism, *Bacillus subtilis*, with only 25% of the ~70 spore coat proteins being conserved between the two organisms, and only 2 of 9 coat assembly (morphogenetic) proteins defined in *B. subtilis* having homologs in *C. difficile*. We previously identified SipL as a clostridia-specific coat protein essential for functional spore formation. Heterologous expression analyses in *E. coli* revealed that SipL directly interacts with *C. difficile* SpoIVA, a coat morphogenetic protein conserved in all spore-forming organisms, through SipL's C-terminal LysM domain. In this study, we show that SpoIVA-SipL binding is essential for *C. difficile* spore formation and identify specific residues within the LysM domain that stabilize this interaction. Fluorescence microscopy analyses indicate that binding of SipL's LysM domain to SpoIVA is required for SipL to localize to the forespore, while SpoIVA requires SipL to promote encasement of SpoIVA around the forespore. Since we also show that clostridial LysM domains are functionally interchangeable at least in *C. difficile*, the basic mechanism for SipL-dependent assembly of clostridial spore coats may be conserved.

Importance

The metabolically dormant spore-form of the major nosocomial pathogen, *Clostridioides difficile*, is its major infectious particle. However, the mechanisms controlling the formation of these resistant cell types are not well understood, particularly with respect to its outermost layer, the spore coat. We previously identified two spore morphogenetic proteins in *C. difficile*: SpoIVA, which is conserved in all spore-forming organisms, and SipL, which is conserved only in the Clostridia. Both SpoIVA and SipL are essential for heat-resistant spore formation and directly interact through SipL's C-terminal LysM domain. In this study, we demonstrate that the LysM domain is critical for SipL and SpoIVA function, likely by helping recruit SipL to the forespore during spore morphogenesis. We further identified residues within the LysM domain that are important for binding SpoIVA and thus functional spore formation. These findings provide important insight into the molecular mechanisms controlling the assembly of infectious *C. difficile* spores.

Introduction

The Gram-positive pathogen *Clostridioides* (formerly *Clostridium*) *difficile* is a leading cause of antibiotic-associated diarrhea and gastroenteritis in the developed world (1, 2). Since *C. difficile* is an obligate anaerobe, its major infectious particle is its aerotolerant, metabolically dormant spore form (3, 4). *C. difficile* spores in the environment are ingested by susceptible hosts and transit through the gastrointestinal tract until they sense specific bile salts in the small intestine that trigger spore germination (5). The germinating spores outgrow into vegetative cells in the large intestine, which then produce the glucosylating toxins responsible for disease symptoms (6). A subset of these vegetative cells will initiate the developmental program of sporulation, producing the infectious spores needed for this organism to survive exit from the host (7, 8).

The basic architecture of spores is conserved across endospore-forming bacteria: a central core consisting of partially dehydrated cytosol is surrounded by a protective layer of modified peptidoglycan called the cortex, which is in turn encased by a series of proteinaceous shells known as the coat (9). The cortex is critical for maintaining spore dormancy and conferring resistance to heat and ethanol, while the coat acts as a molecular sieve that protects the spore from enzymatic and oxidative insults (9-11). The cortex is assembled on top of the thin layer of vegetative cell wall that is sandwiched in between two membranes known as the inner forespore and outer forespore membranes. The outer forespore membrane derives from the mother cell and encases the developing forespore during engulfment by the mother cell. During this time, a series of self-polymerizing proteins will assemble on the outer forespore-membrane and eventually form the concentric layers of protein that define the spore coat (10).

The mechanisms controlling coat assembly have been studied for decades in *Bacillus subtilis*, where the key coat morphogenetic proteins that control the recruitment and assembly of the coat layers have been identified (10, 12). The innermost layer, known as the basement layer, is formed through the coordinated actions of SpoVM, SpoIVA, and SpoVID. SpoVM is a small amphipathic helix that embeds itself in the forespore membrane (13) and directly interacts with SpoIVA (14), facilitating SpoIVA's assembly around the forespore (14). SpoIVA is a self-polymerizing ATPase (15) that binds SpoVM through residues in SpoIVA's C-terminal region (14). In the absence of SpoVM, SpoIVA forms a single focus on the forespore and fails to encase the forespore (14, 16). SpoIVA also recruits SpoVID to the forespore (17), and their interaction promotes the encasement of both proteins around the forespore (17).

Loss of any one of these coat morphogenetic proteins in *B. subtilis* prevents recruitment of additional coat proteins to the forespore and causes the polymerized coat to mislocalize to the mother cell cytosol, at least in the case of *spoIVA* (18) and *spoVID* (19) mutants. Loss of either SpoIVA or SpoVM prevents cortex assembly and thus heat-resistant spore formation (~10^{-8} defect) due to activation of a quality control pathway conserved in the Bacilli (18, 20, 21). In contrast, loss of SpoVID results in only an ~10-fold defect in heat-resistant spore formation but an ~1000-fold decrease in lysozyme resistance, consistent with the presence of the cortex layer in a *spoVID* mutant (19). It should be noted that a more recent study observed that the lysozyme sensitivity of a clean *spoVID* deletion mutant is less severe than that of a transposon mutant (~10-fold vs. ~1000-fold) (22).

Interestingly, while SpoIVA and SpoVM appear to be conserved in all spore-forming organisms, SpoVID is conserved only in the Bacilli (23). Of the 9 coat morphogenetic proteins that have been defined in *B. subtilis*, only two have homologs in *C. difficile*, namely SpoIVA and

SpoVM (24). While we previously showed that SpoIVA is critical for spore formation in *C. difficile* (25), we surprisingly found that SpoVM is largely dispensable for functional *C. difficile* spore formation, despite abnormalities in coat adherence to the forespore being observed (26). Furthermore, unlike *B. subtilis*, both *spoVM* and *spoIVA* mutants in *C. difficile* produce cortex (25, 26), although some abnormalities in cortex thickness are observed (26).

Although SpoVID is not conserved in the Clostridia, we previously showed that *C. difficile* produces a functional homolog to SpoVID called SipL (CD3567). Similar to *B. subtilis* SpoVID (17), *C. difficile* SipL is required for proper localization of the coat around the forespore (25), and SipL directly interacts with *C. difficile* SpoIVA (25), even though SipL and SpoVID exhibit no sequence homology outside of their shared C-terminal LysM domain (25) (**Fig. 1A**). However, unlike *B. subtilis* SpoVID, *C. difficile*'s LysM domain directly binds to SpoIVA (25), whereas SpoVID's LysM domain is dispensable for SpoVID binding to SpoIVA (17). Furthermore, loss of *C. difficile* SipL causes a severe heat-resistance defect ($<10^6$) (25), in contrast with the mild defects observed in *B. subtilis spoVID* mutants (19, 22).

While we previously showed that SipL binds to SpoIVA through its LysM domain using a heterologous *E. coli* expression system (25), in this study we tested the hypothesis that this interaction is critical for *C. difficile* spore formation using deletion and co-immunoprecipitation analyses in *C. difficile*. We also identified residues in the LysM domain important for both SipL function and binding to SpoIVA. Lastly, we determined the requirement for the LysM domain to localize SipL to the forespore and the localization dependencies of SpoIVA and SipL.

RESULTS

The LysM domain is required for SipL function.

Based on our prior finding that SipL binding to SpoIVA depends on SipL's LysM domain when heterologously produced in *E. coli* (25), we sought to test whether SipL binding to SpoIVA is critical for SpoIVA and/or SipL function during *C. difficile* sporulation. To this end, we expressed a construct encoding a deletion of the LysM domain in a Δ*sipL* strain we previously constructed (27) to generate strain Δ*sipL/sipL*$_{\Delta lysM}$. As with all constructs tested in this manuscript, the *sipL*$_{\Delta lysM}$ construct was expressed from the native *sipL* promoter from the ectopic *pyrE* locus of 630Δ*erm* background using the *pyrE*-based allele coupled exchange system (28). Functional spore formation in the *sipL*$_{\Delta lysM}$ and wild-type *sipL* complementation strains was then assessed using a heat resistance assay. In this assay, sporulating cultures are heat-treated to kill vegetative cells, while heat-resistant spores in the cultures capable of germinating and forming colonies on plates are enumerated and compared to colony-forming unit (CFU) counts from untreated samples. The LysM domain mutant (Δ*lysM*) was defective in heat-resistant spore formation at levels similar to the parental Δ*sipL* strain (~6-log decrease, **Fig. 1B**). In contrast, the wild-type *sipL* construct expressed from the *pyrE* locus (Δ*sipL*/*sipL*) fully complemented the parental Δ*sipL* strain.

To ensure that the inability of the *sipL*$_{\Delta lysM}$ construct to complement the Δ*sipL* strain was not due to destabilization of SipL$_{\Delta LysM}$, we analyzed SipL levels in the different *sipL* complementation strains using an antibody raised against SipL lacking its LysM domain. These analyses revealed that loss of the LysM domain did not reduce SipL levels in sporulating cells relative to wild-type or the wild-type *sipL* complementation strain (**Fig. 1C**). Thus, the sporulation defect of the Δ*sipL*/*sipL*$_{\Delta lysM}$ strain is because SipL lacking its LysM domain is non-

146 functional. Consistent with our prior finding that SipL helps stabilize SpoIVA (25), SpoIVA
147 levels were slightly reduced in the Δ*sipL* and Δ*sipL*/*sipL*$_{\Delta lysM}$ strains. However, the reduction in
148 SpoIVA levels did not appear as large or as consistent in our analyses of the 630Δ*erm* Δ*sipL*
149 mutants relative to the previously characterized JIR8094 *sipL*::*erm* Targetron mutant (25), which
150 may reflect strain-specific differences between JIR8094 and 630Δ*erm* (29).

151 Phase-contrast microscopy analyses revealed that the Δ*lysM* strain resembled the Δ*sipL*
152 strain in that it failed to produce phase-bright spores (**Fig. 1B**). Instead, these defective strains
153 occasionally produced phase-gray sporelets (orange arrows) (20) that did not achieve the oval
154 shape and phase-bright contrast of wild-type spores (**Fig. 1B**). Furthermore, phase-dark regions
155 (pink arrows) were visible in the mother cell cytosol of Δ*lysM* and Δ*sipL* strains unlike wild type
156 and the wild-type complementation strain. These regions likely correspond to mislocalized spore
157 coat based on prior work (25, 26, 30). To address this possibility, we visualized the spore coat of
158 these strains using transmission electron microscopy (TEM). Δ*sipL*/*sipL*$_{\Delta lysM}$ and Δ*sipL* cells
159 failed to localize coat around the forespore in analyses of >50 sporulating cells. Instead,
160 polymerized coat detached from the forespore and mislocalized to the mother cell cytosol in
161 ~40% of these cells (pink arrow, **Fig. 2**), while polymerized coat appeared to slough off the
162 forespore (previously termed "bearding," (26) yellow arrow, **Fig. 2**) in ~40% of these strains.
163 Neither of these phenotypes was detected in wild type or the wild-type *sipL* complementation
164 strain, where coat was localized around the forespore in ~95% of wild-type and Δ*sipL*/*sipL* cells
165 or otherwise was not yet visible. Taken together, these analyses indicate that loss of SipL's
166 LysM domain results in coat mislocalization and impairs its adherence to the forespore.
167
168 **SipL's LysM domain mediates SipL binding to SpoIVA during *C. difficile* sporulation.**

Since we previously showed that SipL's C-terminal LysM domain is required for SpoIVA to bind to SipL using recombinant proteins produced in *E. coli* (25, 31), we next wanted to confirm that the LysM domain mediates binding to SpoIVA in *C. difficile*. To this end, we compared the ability of C-terminally FLAG-tagged SipL and $SipL_{\Delta LysM}$ to co-immunoprecipitate SpoIVA in sporulating *C. difficile* lysates. In particular, we complemented a Δ*sipL* strain with constructs encoding either wild-type SipL or $SipL_{\Delta LysM}$ carrying C-terminal FLAG epitope-tags (3xFLAG). FLAG-tagged wild-type SipL readily pulled-down SpoIVA from sporulating cell lysates, whereas FLAG-tagged $SipL_{\Delta LysM}$ failed to pull-down SpoIVA (**Fig. 3**). SpoIVA also did not co-immunoprecipitate with untagged SipL variants. Importantly, FLAG-tagged SipL fully restored functional spore formation to the Δ*sipL* background, whereas the FLAG-tagged $SipL_{\Delta LysM}$ failed to complement the Δ*sipL* strain (**Fig. S1**). Taken together, these analyses indicate that SipL binding to SpoIVA depends on SipL's LysM domain in *C. difficile*, and this interaction appears essential for functional spore formation.

Clostridial $SipL_{LysM}$ domains can functionally substitute for the *C. difficile* $SipL_{LysM}$ domain

We next sought to identify key residues within SipL's LysM domain that are required for the SpoIVA-SipL interaction and thus SipL function. To facilitate the identification of these residues, we tested whether LysM domains from closely related clostridial SipL homologs and SipL's functional homolog, *B. subtilis* SpoVID (17, 25, 32), could replace the *C. difficile* $SipL_{LysM}$ domain (**Fig. 4A**). Constructs encoding LysM domain chimeras from *Paraclostridium sordellii* and *Paraclostridium bifermentans* SipL homologs (~60% identity and 80% similarity

192 with the *C. difficile* $SipL_{LysM}$ domain), *Clostridium perfringens* SipL (39% identity and 57%
193 similarity), and *B. subtilis* SpoVID (23% identity but 55% similarity) were constructed and used
194 to complement a *C. difficile* Δ*sipL* strain. *P. sordellii* and *P. bifermentans* are members of the
195 same Peptostreptococcaceae family as *C. difficile* (33) but part of a different genus (34), while *C.*
196 *perfringens* is part of the *Clostridium* genus in the Clostridiaceae family.

197 Δ*sipL* strains complemented with the clostridial chimeras (Δ*sipL/sipL-lysM*$_{bif}$,
198 Δ*sipL/sipL-lysM*$_{sor}$, and Δ*sipL/sipL-lysM*$_{per}$) were indistinguishable from wild type and the wild-
199 type *sipL* complementation strain (Δ*sipL/sipL*) by phase-contrast microscopy, since a mixture of
200 phase-bright spores (blue arrows), phase-bright (yellow arrows), and phase-gray (green arrows)
201 forespores were visible in all strains producing clostridial LysM domains (**Fig. S2A**). In contrast,
202 the *B. subtilis* chimera resembled the Δ*sipL/sipL*$_{\Delta lysM}$ strain, with no phase-bright spores being
203 detected and most of the forespores being phase-dark or phase-gray sporelets (orange arrows).
204 Similar to the parental Δ*sipL* strain, mislocalized coat was visible in the cytosol of the *B. subtilis*
205 LysM chimera strain (pink arrows, **Fig. S2A**).

206 Consistent with these observations, the clostridial $SipL_{LysM}$ domain swap constructs fully
207 complemented the Δ*sipL* strain in heat resistance assays (**Figs. 4A** and **S2A**), whereas the *B.*
208 *subtilis* LysM chimeric strain failed to produce heat-resistant spores like the parental Δ*sipL*
209 strain. Importantly, western blotting revealed that the different chimeric SipL variants were
210 produced at relatively similar levels as *C. difficile* SipL using an antibody raised against
211 $SipL_{\Delta LysM}$ (**Fig. S2B**), although slightly lower levels of SipL carrying the *B. subtilis* SpoVID
212 LysM domain were observed. Taken together, these results suggest that clostridial $SipL_{LysM}$
213 domains can still bind *C. difficile* SpoIVA, whereas the *B. subtilis* $SpoVID_{LysM}$ domain cannot.
214

215 **Identification of *C. difficile* LysM domain residues important for SipL function**

216

217 We next used these observations to guide finer-scale chimeric analyses of the *C. difficile*
218 LysM domain by identifying differences between the sequences of the clostridial $SipL_{LysM}$
219 domains and the *B. subtilis* SpoVID LysM domain. Clostridial LysM domains exhibited the
220 greatest sequence similarity in the N-terminal portion of the LysM domain, so we swapped the
221 residues corresponding to 463-482 of *C. difficile*'s $SipL_{LysM}$ domain with those of the *B. subtilis*
222 SpoIVD LysM domain (Region A, **Fig. 4A**). We also assessed the importance of the C-terminus
223 of the LysM domain by swapping out residues 483-516 (Region E). While the C-terminal
224 chimeric construct, $sipL_{483\text{-}516}$, fully complemented the Δ*sipL* strain, the $sipL_{463\text{-}482}$ chimeric
225 construct resulted in an ~3000-fold decrease in heat resistance efficiency relative to wild type
226 and the wild-type *sipL* complementation construct (**Fig. 4B**, $p < 0.001$). Given the apparent
227 importance of region A, we generated constructs encoding smaller scale swaps, namely residues
228 463-476 (Region B), 475-476 (Region C), and 478-480 (Region D). Swapping the residues in
229 Regions B and C resulted in an ~100-fold decrease in heat resistance efficiency relative to wild
230 type, while the Region D swap construct resulted in an ~20-fold decrease relative to wild-type
231 (**Fig. 4B**, $p < 0.01$). Importantly, all the SipL chimeric variants generated produced SipL at wild-
232 type or close to wild-type levels (**Fig. 4B**), consistent with our earlier analyses of the Δ*lysM*
233 strain (**Fig. 1C**).

234 Based on these findings, we next constructed individual point mutations in Regions C and
235 D. Region C comprises residues Trp475 and Asn476 in *C. difficile* SipL, which are glutamate
236 and arginine residues, respectively, in the LysM domain of *B. subtilis* SpoVID. We mutated
237 Trp475 to glutamate, since these residues differ more in size and charge than Asn476 relative to

arginine. Expression of the *sipL*$_{W475E}$ in Δ*sipL* resulted in a similar ~100-fold defect in heat-resistant spore formation (**Fig. 5A**) relative to wild type as the *sipL*$_{475-476}$ Region B allele, suggesting that the substitution of Trp475 for Glu (W475E) is the major contributor to the sporulation defect of the Region B mutant.

By phase-contrast microscopy, the *sipL*$_{W475E}$ strain resembled the Δ*sipL* strain in producing cells with mislocalized coat (**Fig. 5C**). However, the coat did not appear to be as detached from the forespore of W475E mutant cells relative to the parental Δ*sipL* strain (pink arrows, **Fig. 5C**). Furthermore, W475E produced phase-bright sporelets (purple arrows) as opposed to the phase-gray sporelets (orange arrows) of the parental Δ*sipL* strain.

To further assess the importance of the Trp475 residue for *C. difficile* SipL function, we mutated this residue to the small, uncharged residue, alanine (W475A), and the neutral, aromatic residue, phenylalanine (W475F). We also tested whether reducing the size of the negatively-charged residue by introducing an aspartate at residue 475 instead of a glutamate would affect SipL function. While the conservative change, W475F, did not reduce SipL function, both the W475A and W475D mutations decreased heat-resistant spore formation to levels similar to the W475E mutant (**Fig. 5A**). Since these strains also produced phase-bright sporelets and partially displaced coat (**Fig. 5C**∫ like the W475E mutant, these results suggest that the aromatic nature of Trp475 is critical to its function.

We next tested whether a single point mutation in region D, which consists of three residues from 478 to 480, could recapitulate the ~20-fold decrease in heat resistance observed for the region D swap mutant relative to wild type (**Fig. 4**). We focused on lysine 479 in *C. difficile* LysM, since this residue is a lysine in clostridial SipL$_{LysM}$ domains but a negatively-charged glutamate residue in the *B. subtilis* SpoVID LysM domain, and the other two residues in this

region carried more conservative changes of alanine 478 to cysteine and lysine 480 to arginine. Substitution of lysine 479 to glutamate did not impair the ability of this allele to complement Δ*sipL* (K479E, **Fig. S3**), suggesting that the other changes in region D could be responsible for the ~20-fold defect observed with this chimeric mutant. However, since the defect was relatively mild relative to region B, we did not further analyze point mutants in this region.

To assess whether additional residues in Region B (463-482) might also contribute to SipL function, we constructed the following point mutant alleles based on differences between the LysM domains of *C. difficile* SipL and *B. subtilis* SpoVID: Y466C, G471E, and N482E. We also tested a few other residues just outside Region B: T483I and E485S. These mutant constructs all fully complemented Δ*sipL* (**Fig. S3**), suggesting that these individual residues do not affect SipL binding to SpoIVA.

We next analyzed the contribution of the first residue of *C. difficile*'s $SipL_{LysM}$ domain because two observations suggested that Ile463 may be important for SipL binding to SpoIVA. Although SipL's LysM domain is annotated in the NCBI as spanning residues 464-508, we previously observed that a His-tagged construct encoding residues 464 to 516 failed to bind SpoIVA in co-affinity purification analyses in *E. coli*, whereas a construct spanning residues 463-516 resulted in robust pull-down (25). Furthermore, when we tested LysM chimeras using the NCBI-annotated LysM domains of clostridial SipL homologs, all these constructs failed to complement Δ*sipL* (data not shown). However, inclusion of the equivalent Ile463 residue allowed for full complementation (**Fig. 4A**). Taken together, these observations strongly suggest that Ile463 is important for SipL function.

Since Ile463 is a methionine in *B. subtilis* SpoVID, we tested whether the identity and/or precise position of residue 463 is critical for SipL function. Specifically, we generated

284 complementation constructs in which Ile463 was either deleted (ΔI463) or mutated to *B. subtilis*
285 SpoVID's methionine (I463M), negatively-charged glutamate (I463E), or positively-charged
286 arginine (I463R). No heat-resistant spores were detected when Ile463 was deleted (**Fig. 5B**),
287 consistent with our observations with the chimeric LysM constructs (data not shown). In
288 contrast, *sipL*$_{I463M}$, the *B. subtilis* SpoVID LysM point mutation, fully complemented the Δ*sipL*
289 mutant (**Fig. 5B**). These results indicate that the sequence difference at residue 463 between the
290 *C. difficile* and *B. subtilis* LysM domains is not responsible for the failure of the SpoVID LysM
291 domain to complement for SipL function. Similarly, only a slight decrease in heat-resistant spore
292 formation was observed with the *sipL*$_{I463E}$ mutation (**Fig. 5B**). In contrast, the *sipL*$_{I463R}$ mutation
293 decreased spore formation by ~9-fold ($p < 0.03$, **Fig. 5B**), indicating that a positively charged
294 residue at position 463 can impair SipL function.

295 Phase-contrast microscopy analyses revealed that the I463R mutant produced phase-
296 bright sporelets and partially displaced coat similar to the W475 mutants (**Fig. 5C**), a phenotype
297 that appears to be less severe than loss of SipL or the LysM domain altogether (**Figs. 1B** and **S2**).
298 Indeed, the sipL$_{ΔI463}$ strain resembled the parental Δ*sipL* strain in that only phase-gray sporelets
299 (purple arrows, **Fig. 5C**) were observed, and the coat displacement appeared more severe than
300 the W475 and I463R point mutant strains (pink arrows). Taken together, our results suggest that
301 the spacing of the LysM domain, i.e. starting at position 463, is critical for SipL function, while
302 the chemical identity of the residue at this position can also impact SipL function.
303
304 **Isoleucine 463 and Tryptophan 475 enhance binding of SipL to SpoIVA**
305

306 The decreased ability of *sipL* constructs encoding mutations in either Ile463 or Trp475 to
307 complement Δ*sipL* implied that point mutations in these residues decrease SipL binding to
308 SpoIVA. To test this hypothesis, we generated constructs encoding FLAG-tagged SipL that carry
309 mutations in these residues and measured their ability to pull-down SpoIVA in co-
310 immunoprecipitation analyses. Whereas SpoIVA was readily pulled-down by FLAG-tagged
311 wild-type SipL, no SpoIVA was detected in immunoprecipitations with SipL variants where
312 Ile463 was either deleted (ΔI463) or mutated to arginine (I463R, **Fig. 5D**). Reduced amounts of
313 SpoIVA were pulled down with the FLAG-tagged $SipL_{W475E}$ variant relative to wild type.
314 Interestingly, the pull-down results did not entirely match the severity of the mutations, since the
315 $sipL_{W475E}$ allele resulted in an ~100-fold heat resistance defect, but the $sipL_{I463R}$ allele caused
316 only a ~9-fold heat resistance defect. This result suggests that even though SpoIVA can bind
317 $SipL_{W475E}$, the interaction does not result in optimal SpoIVA and/or SipL function.
318
319 **SipL localization to the forespore depends on the LysM domain.**
320
321 Since SpoIVA binding to SipL's LysM domain appears critical for these proteins to
322 mediate spore formation, we hypothesized that SipL's LysM domain would be important for
323 recruiting SipL to the forespore and allowing it to encase the forespore. To directly test this
324 hypothesis, we complemented Δ*sipL* with a construct encoding an mCherry fusion to $SipL_{\Delta LysM}$.
325 Whereas wild-type SipL fused to mCherry encases the forespore (**Fig. 6A**) as previously reported
326 (27), deletion of the LysM domain prevented $SipL_{\Delta LysM}$-mCherry localization to the forespore,
327 since the $SipL_{\Delta LysM}$-mCherry signal was largely distributed in the mother cell cytosol (**Fig. 6A**).
328 Western blot analyses revealed that mCherry was not liberated from $SipL_{\Delta LysM}$-mCherry (**Fig.**

S4A), indicating that SipL's LysM domain directs SipL to the forespore and allows it to encase the forespore, presumably through its interaction with SpoIVA.

SipL requires SpoIVA to localize to and encase the forespore and encase it, while SpoIVA requires SipL to encase the forespore.

To directly assess whether SpoIVA was required for SipL to localize to the forespore, we analyzed the localization of SipL-mCherry in a Δ*spoIVA*Δ*sipL* mutant. It was necessary to use the double mutant because the presence of wild-type (untagged) SipL results in some SipL-mCherry being re-distributed to the cytosol (data not shown). In the absence of SpoIVA, the SipL-mCherry signal was entirely cytosolic similar to the localization pattern of $SipL_{\Delta LysM}$-mCherry (**Fig. 6A**), although the cytosolic SipL-mCherry signal appeared more intense in the absence of SpoIVA.

Since these results indicated that SipL localization to and around the forespore depends on SpoIVA through its interaction with SipL's LysM domain, we next assessed whether SpoIVA's localization around the forespore (26) depends on SipL. To test this question, we analyzed the localization of mCherry-SpoIVA, which has almost wild-type function (26), in the absence of SipL. For these experiments, mCherry-SpoIVA localization was analyzed in the presence of wild-type SpoIVA because mCherry-SpoIVA exhibits reduced encasement of the forespore if it is the only variant of SpoIVA present (26). While mCherry-SpoIVA encased the forespore (with some cytosolic localization) when produced in a wild-type strain background, mCherry-SpoIVA produced in the absence of SipL localized to a single, albeit dim, focus on the forespore at the mother cell proximal side (**Fig. 6B**). Notably, the amount of mCherry-SpoIVA

352 produced in the Δ*sipL* background was reduced relative to the wild-type background (**Fig. S4**),
353 consistent with our original finding that SpoIVA levels are reduced in the absence of SipL (25).
354 Taken together, our results indicate that SpoIVA-SipL binding is needed to not only bring SipL
355 to the forespore but also for SipL to encase the forespore; in contrast, SpoIVA can find the
356 forespore in the absence of SipL, but SpoIVA requires SipL to surround the forespore.
357
358 **Discussion**
359
360 In this study, we show that the LysM domain of *C. difficile* SipL is critical for functional
361 spore formation because it binds to SpoIVA and allows both these proteins to encase the
362 developing forespore. Our conclusions are based on the following observations: (i) SipL-
363 mCherry mislocalizes to the cytosol if either SpoIVA or SipL's LysM domain is absent (**Fig. 6**);
364 (ii) deletion of the LysM domain results in coat mislocalization to the mother cell cytosol (**Fig.**
365 **2**) and prevents heat-resistant spore formation (**Fig. 1**) analogous to the *sipL* deletion mutant, and
366 SpoIVA cannot bind to SipLΔ_{LysM} in immunoprecipitation analyses (**Fig. 3**); and (iii) specific
367 point mutations in SipL's LysM domain impair binding to SpoIVA and reduce functional spore-
368 formation (**Fig. 5**).
369 Through chimeric LysM analyses that exploited the failure of the *B. subtilis* SpoVID
370 LysM domain to complement *C. difficile* LysM domain function (**Fig. 4**), we identified two point
371 mutations in the LysM domain, W457E and I463R, that decrease heat-resistant spore formation
372 by decreasing or even preventing binding to SpoIVA (**Fig. 5**). While these mutations reduced
373 spore formation by ~100- and 10-fold, respectively, their effects on coat mislocalization were
374 qualitatively less severe. The coat in *sipL*$_{W475E/D/A}$ and *sipL*$_{I463R}$ mutants appeared more closely

associated with the forespore in these strains, particularly if the forespores/sporelets appeared phase-bright (**Fig. 5C**). In contrast, the coat appeared to be more frequently displaced to the mother cell cytosol in *sipL* mutants carrying non-functional *sipL* alleles, like Δ*lysM*, *sipL*$_{\Delta I463}$, and *sipL-lysM*$_{Bsub}$ (**Figs. 1, 5**, and **S2**). Indeed, the *sipL* strains that failed to produce heat-resistant spores did not make the phase-bright, swollen sporelets observed in *sipL*$_{W475E/D/A}$ and *sipL*$_{I463R}$ mutants (**Fig. 5C**, purple arrows). It would be interesting to test whether the *sipL*$_{W475E/D/A}$ and *sipL*$_{I463R}$ mutants localize coat close to the forespore because SipL$_{W457E/D/A}$ and SipL$_{I463R}$ variant can still localize to the forespore and/or partially encase the forespore. This scenario seems possible for the *sipL*$_{W457E}$ allele, since SipL$_{W475E}$ partially binds SpoIVA (**Fig. 5D**).

Our analyses also implicated the first residue of the LysM domain as being important for SipL function. The I463R mutation, but not the I463M or I463E mutations, significantly impaired SipL function, while deletion of the Ile463 residue altogether completely abrogated SipL function (**Fig. 5**). These observations suggest that Ile463 is needed as a linker between the LysM domain and the rest of the SipL protein, or it could be needed for proper folding of the LysM domain. This latter possibility seems less likely given that Ile463 is not strongly conserved at this position across LysM domains (**Fig. S5**) and does not appear to play an important structural role in the LysM domains whose structures have been solved (35).

LysM domains frequently bind to N-acetylglucosamine (NAG) residues in chitin (e.g. in eukaryotic LysM domains) and peptidoglycan in prokaryotic LysM-containing proteins (35, 36). Recent structural analyses have revealed the molecular basis for LysM binding to peptidoglycan (36). Interestingly, some of the residues identified as being critical for recognizing NAG in an *Enterococcus faecalis* LysM domain are not conserved in the four clostridial SipL$_{LysM}$ domains

analyzed in this study (**Fig. S5A**, red asterisks), although they typically have similar properties in clostridial LysM domains. Nevertheless, when the structure of *C. difficile* $SipL_{LysM}$ domain is predicted using the iTasser algorithm (37), it aligns closely with the structures of several LysM domains (**Fig. S5B**), raising the possibility that $SipL_{LysM}$ domains can bind peptidoglycan.

While this possibility remains to be tested, we note that the *B. subtilis* $SpoVID_{LysM}$ domain does not bind peptidoglycan even though putative peptidoglycan-binding residues are conserved (32). In contrast, the LysM domain of SafA, a coat morphogenetic protein that modulates inner coat assembly downstream of SpoVID (38, 39), functions both as a protein-protein interaction module and a peptidoglycan binding domain (32). Specifically, SafA's LysM domain binds to SpoVID early during coat morphogenesis, while later during morphogenesis, SafA's LysM domain binds to the spore cortex, the modified peptidoglycan layer that confers heat resistance to spores (32). Thus, even though SafA lacks a transmembrane domain to span the outer forespore membrane, its N-terminal LysM domain apparently binds the spore cortex, since SafA exhibits aberrant localization in cortex biogenesis mutants (32). It remains unclear how SafA binding switches from SpoVID to the cortex during spore formation, but a similar event would need to occur if *C. difficile* SipL's LysM domain binds SpoIVA and then to the cortex region. Directly testing whether clostridial $SipL_{LysM}$ domains can bind peptidoglycan would provide important insight to these questions.

Interestingly, in the structure model generated by iTasser (**Fig. S5B**), the Trp457 residue we identified as being important for SipL to bind SpoIVA (**Fig. S5B**) is predicted to be surface-exposed. Thus, Trp457 would appear to be available to directly interact with as-yet-undefined regions of SpoIVA and possibly also to bind cortex peptidoglycan. Future studies directed at identifying regions with SpoIVA that mediate binding to SipL will provide important insight into

421 how the interaction between these two proteins allows for functional spore formation. Given that
422 our results indicate that SpoIVA encasement of the forespore (**Fig. 6**) depends on SipL, it is
423 possible that SipL binding to SpoIVA promotes SpoIVA polymerization. Alternatively, reduced
424 levels of mCherry-SpoIVA in the Δ*sipL* strain may prevent self-polymerization of SpoIVA (40)
425 and thus prevent encasement. Determining the precise effects of SipL binding to SpoIVA on
426 SpoIVA's presumed ATPase and polymerization activities will provide critical insight into how
427 infectious *C. difficile* spores are built and could guide efforts to prevent spore formation by
428 clostridial pathogens.
429
430 **Figure Legends**
431
432 **Figure 1. The LysM domain of *C. difficile* is essential for spore formation**. (A) Schematic of
433 *C. difficile* SipL domain structure. SipL contains three domains of unknown function (DUF3794)
434 and a C-terminal LysM domain. (B) Phase-contrast microscopy analyses of the indicated *C.*
435 *difficile* strains ~20 hrs after sporulation induction. Δ*sipL* was complemented with either the
436 wild-type allele or one encoding a deletion of the LysM domain (Δ*sipL*/*sipL*$_{\Delta lysM}$). Arrows mark
437 examples of sporulating cells at different stages of maturation: blue arrows highlight phase-
438 bright free spores; yellow arrows mark mature phase-bright forespores, which are formed
439 following cortex formation (22, 24); green arrows highlight immature phase-dark forespores;
440 orange arrows highlight phase-gray sporelets, which produce a phase-dark ring surrounding the
441 forespore but do not become phase-bright; and pink arrows demarcate regions suspected to be
442 mislocalized coat based on previous studies (26, 30). Heat resistance efficiencies were
443 determined from 20-24 hr sporulating cultures and represent the mean and standard deviation for

444 a given strain relative to wild type based on a minimum of three independent biological
445 replicates. Statistical significance relative to wild type was determined using a one-way ANOVA
446 and Tukey's test. Scale bar represents 5 µm. The limit of detection of the assay is 10^{-6}. (C)
447 Western blot analyses of SipL, SpoIVA, and Spo0A. SipL was detected using an antibody raised
448 against SipL lacking its LysM domain (i.e. $SipL_{\Delta LysM}$). Asterisks indicate non-specific bands
449 detected by the $SipL_{\Delta LysM}$ antibody. SpoIVA levels were analyzed because of the prior finding
450 that SpoIVA levels are reduced in the absence of SipL (25). Modest decreases in SipL levels
451 were observed in the Δ*sipL* and Δ*sipL*/$sipL_{\Delta lysM}$ strains. Spo0A was used as a proxy for
452 measuring sporulation induction (4, 25). The western blots shown are representative of the
453 results of three independent biological replicates.
454
455 **Figure 2. Loss of SipL's LysM domain results in coat mislocalization defects**. (A)
456 Transmission electron microscopy (TEM) analyses of wild-type 630Δ*erm,* Δ*sipL*, and Δ*sipL*
457 complemented with either wild-type *sipL* or *sipL* encoding a LysM deletion ($sipL_{\Delta lysM}$) after 23
458 hrs of sporulation induction. Scale bars represent 500 nm. Blue arrows mark properly localized
459 coat, i.e. surrounding the entire forespore (FS), whereas pink arrows mark coat that has
460 completely detached from the forespore and is found exclusively in the mother cell (MC)
461 cytosol. Yellow arrows mark cells where coat appears to be detaching from the forespore but
462 remains partially associated, also known as "bearding" (26). The percentages shown are based on
463 analyses of at least 50 cells for each strain with visible signs of sporulation from a single
464 biological replicate.
465

Figure 3. The LysM domain is required for SipL to bind SpoIVA in sporulating *C. difficile* cultures. FLAG-tagged SipL was immunoprecipitated from cleared lysates prepared from the indicated *C. difficile* Δ*sipL* complementation cultures ("Input" fraction) using anti-FLAG magnetic beads. Proteins bound to the beads after several washes were eluted using FLAG peptide ("Elution" fraction). "WT" indicates that Δ*sipL* was complemented with the wild-type *sipL* allele, whereas "Δ*lysM*" indicates that Δ*sipL* was complemented with a $sipL_{\Delta lysM}$ construct. "FLAG-tagged" indicates that the complementation constructs encoded a C-terminal FLAG tag consisting of three successive FLAG tags, which resulted in the SipL-FLAG fusions exhibiting a higher mobility during SDS-PAGE. The untagged *sipL* complementation strains served as negative controls to ensure that untagged SipL and SpoIVA were not non-specifically pulled-down by the anti-FLAG beads. Sporulation was induced for 24 hrs before lysates were prepared. The immunoprecipitations shown are representative of three independent biological replicates.

Figure 4. Chimeric analyses identify a small region of the LysM domain important for SipL function. (A) Alignment of LysM domains from SipL homologs from *C. difficile* (CAJ70473), *P. bifermentans* (EQK49575), *P. sordellii* (EPZ54296), and *C. perfringens* (YP_696893), as well as the LysM domain from *B. subtilis* SpoVID (NP_390689). Blue boxes with white text indicate residues that are completely conserved; green boxes indicate residues that are conserved in some of the homologs; and yellow boxes mark residues that are similar between the homologs. The brackets and letters below the alignment indicate the regions swapped between the *C. difficile* SipL and *B. subtilis* SpoVID LysM domains. The red asterisks highlight residues whose mutations impaired functional spore formation, while black asterisks indicate residues whose mutation to the residue in the *B. subtilis* SpoVID LysM domain did not reduce SipL function, i.e.

spore formation (**Fig. S3**). (B) Graphical representation of the heat resistance assay results and western blot analyses of SipL in the chimeric constructs in (A) using an antibody raised against SipL lacking the LysM domain. *sipL*^{C} refers to the Δ*sipL/sipL* wild-type complementation strain. Asterisk marks a non-specific band detected by the anti-SipL$_{\Delta LysM}$ antibody. Spo0A was used as a proxy for measuring sporulation induction (4, 25). The western blots shown are representative of the results of three independent biological replicates. The heat resistance efficiencies for all chimeric swaps were determined from 20-24 hr sporulating cultures and represent the mean and standard deviation for a given strain relative to wild type based on a minimum of three independent biological replicates. Statistical significance relative to wild type was determined using a one-way ANOVA and Tukey's test. ** $p < 0.01$.

Figure 5. Identification of LysM domain residues required for optimal SipL function. Western blot analyses of strains encoding SipL point mutations in Trp475 (A) and Ile463 (B) using an antibody raised against SipL lacking the LysM domain. Asterisk marks the non-specific band detected by the anti-SipL$_{\Delta LysM}$ antibody. Spo0A was used as a proxy for measuring sporulation induction (4, 25). The western blots shown are representative of the results of three independent biological replicates. Heat resistance efficiencies were determined from 20-24 hr sporulating cultures and represent the mean and standard deviation for a given strain relative to wild type based on a minimum of three independent biological replicates. The limit of detection of the assay is 10^{-6}. Statistical significance relative to wild type was determined using a one-way ANOVA and Tukey's test. ** $p < 0.01$, * $p < 0.05$. (C) Phase-contrast microscopy analyses of the indicated *C. difficile* strains ~20 hrs after sporulation induction. Δ*sipL* was complemented with either the wild-type allele or the indicated LysM domain mutations. Arrows mark examples

of sporulating cells with various defects in maturation: orange arrows highlight phase-gray sporelets (20), which produce a phase-dark ring surrounding the forespore but do not become phase-bright; purple arrows highlight phase-bright sporelets that appear swollen but are outlined by a phase-dark ring; and pink arrows demarcate regions likely to be mislocalized coat (26, 30). The images shown derive from two separate experiments, with the Trp475 and Ile463 variants being performed on different days. (D) Co-immunoprecipitations of FLAG-tagged SipL variants carrying either point mutations in the LysM domain (W475E or I463R) or lacking residue Ile463 (ΔI463). Strains containing untagged SipL were used as negative controls to assess the specificity of the SpoIVA co-immunoprecipitations.

Figure 6. SipL binding to SpoIVA is required to localize SipL to the forespore, while SpoIVA encasement of the forespore depends on SipL. (A) Fluorescence microscopy analyses of either Δ*sipL* or Δ*sipL*Δ*spoIVA* complemented with constructs encoding either SipL-mCherry or $SipL_{\Delta LysM}$-mCherry after 20-23 hrs post-sporulation induction. (B) mCherry-SpoIVA localization in either the wild-type or Δ*sipL* strain backgrounds. A wild-type copy of *spoIVA* was present in both strains because the fusion protein does not efficiently encase the forespore unless a wildtype copy of *spoIVA* is present (26). Cells were visualized using phase-contrast (phase) microscopy, and the nucleoid was visualized using Hoechst staining (41). The Hoechst-stained nucleoid is shown in blue, and mCherry fluorescence is shown in red. Engulfment completion excludes Hoechst from staining the forespore (41). The merge of Hoechst and mCherry is also shown. Yellow arrows mark single, dim foci of mCherry-SpoIVA observed in the Δ*sipL* strain background. The images shown are representative of three independent biological replicates.

Materials and Methods

Bacterial strains and growth conditions. 630Δ*erm*Δ*pyrE* (28) was used as the parental strain for *pyrE*-based allele-coupled exchange (ACE, (28)). *C. difficile* strains are listed in **Table S1** and were grown on BHIS agar (42) supplemented with taurocholate (TA, 0.1% w/v; 1.9 mM), kanamycin (50 µg/mL), and cefoxitin (8 µg/mL) as needed for conjugations. *C. difficile* defined media (CDDM, (43)) was used for isolating complementation strains (28). 5-fluoroorotic acid (5-FOA) at 2 mg/mL and uracil at 5 µg/mL as needed for ACE. Cultures were grown under anaerobic conditions using a gas mixture containing 85% N_2, 5% CO_2, and 10% H_2.

Escherichia coli strains for HB101/pRK24-based conjugations and BL21(DE3)-based protein production are listed in **Table S1**. *E. coli* strains were grown at 37˚C, shaking at 225 rpm in Luria-Bertani broth (LB). The media was supplemented with chloramphenicol (20 µg/mL) and ampicillin (50 µg/mL) as needed.

***E. coli* strain construction**. All primers are listed in **Table S2**, and all g-blocks used for cloning are listed in **Table S3**. Details of *E. coli* strain construction are provided in the **Supplementary Text S1**. All plasmid constructs were cloned into DH5α and sequenced confirmed using Genewiz. Plasmids to be conjugated into *C. difficile* were transformed into HB101/pRK24, while the plasmid used for antibody production was transformed into BL21(DE3).

***C. difficile* strain complementation**.

Allele-coupled exchange (ACE, (28)) was used as previously described (44) to construct the Δ*spoIVA*Δ*sipL*Δ*pyrE* double mutant. Δ*spoIVA*Δ*pyrE* was used as the parental strain, with

558 strain #1704 pMTL-YN3 Δ*sipL* being used to introduce the *sipL* mutation. pMTL-YN1C-based
559 complementation constructs were conjugated into Δ*sipL*Δ*pyrE* as previously described (44). Two
560 independent clones of each complementation strain were phenotypically characterized.
561
562 **Plate-based Sporulation**. *C. difficile* strains were grown from glycerol stocks overnight on
563 BHIS plates containing TA (0.1% w/v). Colonies from these cultures were then used to inoculate
564 liquid BHIS cultures, which were grown to stationary phase and then back-diluted 1:50 into
565 BHIS. When the cultures reached an OD_{600} between 0.35 and 0.7, 120 µL was removed to
566 inoculate 70:30 agar plates ((25)). Sporulation was induced on this media for 20-24 hrs. The ~20
567 hr timepoint was used to analyze cultures by phase-contrast microscopy and harvest samples for
568 Western blot analyses.
569
570 **Heat resistance assay on sporulating cells**. Heat-resistant spore formation was measured in
571 sporulating *C. difficile* cultures after 20-24 hrs as previously described (45). Briefly, sporulating
572 cultures were divided into two, with one culture being heat-treated at 60˚C for 30 min, while the
573 second half was left untreated. The samples were serially diluted and plated on BHIS(TA), and
574 the heat resistance (H.R.) efficiency calculated from the colonies that arose. Specifically, the
575 H.R. efficiency represents the average ratio of heat-resistant cells for a given strain relative to the
576 average ratio determined for wild type based on a minimum of three biological replicates.
577 Statistical significance was determined using a one-way ANOVA and Tukey's test.
578
579 **Antibody production**. The anti-$SipL_{\Delta LysM}$ antibody used in this study was raised against
580 $SipL_{\Delta LysM}$-His_6 in a rabbit by Cocalico Biologicals (Reamstown, PA). The recombinant protein

581 was purified from *E. coli* strain #764 (25) (**Table S1**) using Ni^{2+}-affinity resin as previously
582 described (46).
583 .
584 **TEM analyses**. Sporulating cultures (23 hrs) were fixed and processed for electron microscopy
585 by the University of Vermont Microscopy Center as previously described (25). A minimum of
586 50 full-length sporulating cells were used for phenotype counting.
587
588 **Immunoprecipitation analyses.** Sporulation was induced on 70:30 plates for 24 hrs as
589 described above. Cultures from three 70:30 plates per strain were scraped into 3 x 1 mL of
590 FLAG IP buffer (FIB: 50 mM Tris pH 7.5, 150 mM NaCl, 0.02% sodium azide, 1X Halt
591 protease inhibitor (ThermoScientific)). The cultures were transferred into tubes containing a
592 ~300 µL of 0.1 mm zirconia/silica beads (BioSpec). The cultures were lysed using a FastPrep-
593 24 (MP Biomedicals) for 4 x 60 s at 5.5 M/s, with 5 min cooling on ice between lysis intervals.
594 The tubes were pelleted at 14,500 g for 10 min at 4˚C to pellet beads, unbroken cells/spores, and
595 insoluble material. After washing the tubes with additional FIB, the lysates were pooled and
596 FLAG-conjugated magnetic resin was added. This magnetic resin was generated by incubating
597 Dynabead Protein G (ThermoScientific) with anti-FLAG antibodies (Sigma Aldrich) at room
598 temperature followed by washing. The lysates were incubated with the anti-FLAG resin for 2 hrs
599 at room temperature with rotation. After washing the beads with FIB, FLAG-tagged proteins
600 were eluted using FIB containing 0.1 mg/mL FLAG peptide (Sigma Aldrich). All
601 immunoprecipitations were performed on three independent biological replicates.
602
603 **mCherry fluorescence microscopy**. Live cell fluorescence microscopy was performed using

Hoechst 33342 (Molecular Probes, 15 µg/mL) and mCherry protein fusions. Samples were prepared on agarose pads as previously described (30), and samples were imaged 30 min after harvesting to allow for mCherry fluorescence signal reconstitution in the anaerobically grown bacteria as previously described (27). Briefly, phase-contrast and fluorescence microscopy were performed using a Nikon 60x oil immersion objective (1.4 NA) on a Nikon 90i epifluorescence microscope. A CoolSnap HQ camera (Photometrics) was used to acquire multiple fields for each sample in 12 bit format using NIS-Elements software (Nikon). The Texas Red channel was used to acquire images after a 3-90 ms exposure (90 ms for SipL-mCherry and mCherry-IVA), 50 ms for Hoechst staining, and ~3 ms exposures for phase-contrast microscopy) with 2 x 2 binning. Ten Mhz images were subsequently imported into Adobe Photoshop CC 2015 for minimal adjustments in brightness/contrast levels and pseudocoloring. Localization analyses were performed on three independent biological replicates.

Western blot analyses. Samples for western blotting were prepared as previously described (25). Briefly, sporulating cell pellets were resuspended in 100 µL of PBS, and 50 µL samples were freeze-thawed for three cycles and then resuspended in 100 µL EBB buffer (8 M urea, 2 M thiourea, 4% (w/v) SDS, 2% (v/v) β-mercaptoethanol). The samples were boiled for 20 min, pelleted, re-suspended in the same buffer to maximize protein solubilization, boiled for another 5 min and then pelleted. Samples were resolved on 12% SDS-PAGE gels, transferred to Immobilon-FL PVDF membrane, blocked in Odyssey® Blocking Buffer with 0.1% (v/v) Tween 20. Rabbit anti-$SipL_{\Delta LysM}$ and mouse anti-SpoIVA (47) were used at 1:2,500 dilutions; rabbit anti-mCherry (Abcam) was used at a 1:2,000 dilution; and rabbit or mouse anti-Spo0A (25, 31) was used at a 1:1,000 dilution. IRDye 680CW and 800CW infrared dye-conjugated secondary

627 antibodies were used at a minimum of 1:25,000 dilution, and blots were imaged on an Odyssey
628 LiCor CLx. Western blots were performed on sporulating samples derived from three
629 independent biological replicates.
630

631 **Acknowledgments**

632 We would like to thank N. Bishop and J. Schwarz for excellent assistance in preparing samples
633 for transmission electron microscopy throughout this study; D. Weiss and C. Ellermeier for
634 providing the codon-optimized mCherry construct (48); A. Camilli for access to the Nikon
635 microscope; N. Minton (U. Nottingham) for generously providing us with access to the
636 630Δ*erm*Δ*pyrE* strain and pMTL-YN1C and pMTL-YN3 plasmids for allele-coupled exchange
637 (ACE); M. Dembek for directly providing these materials to us and sharing his specific protocols
638 on ACE.
639

640 Research in this manuscript was funded by Award Number T32AI007329 to M.H.T. and
641 R01AI22232 from the National Institutes of Allergy and Infectious Disease (NIAID) to A.S.
642 A.S. is a Pew Scholar in the Biomedical Sciences supported by The Pew Charitable Trusts and a
643 Burroughs Wellcome Investigator in the Pathogenesis of Infectious Disease supported by the
644 Burroughs Wellcome Fund. The content is solely the responsibility of the author(s) and does not
645 necessarily reflect the views of the Pew Charitable Trusts, Burroughs Wellcome, NIAID, or the
646 National Institutes of Health. The funders had no role in study design, data collection and
647 interpretation, or the decision to submit the work for publication.
648

649 A.S. has a paid consultancy for BioVector, Inc., a diagnostic start-up.

650
651 **References**
652
653 1. Freeman J, Bauer M, Baines S, Corver J, Fawley W, Goorhuis B, Kuijper E, Wilcox M.
654 2010. The changing epidemiology of Clostridium difficile infections. Clinical
655 microbiology reviews 23:529-549.
656 2. Lessa FC, Mu Y, Bamberg WM, Beldavs ZG, Dumyati GK, Dunn JR, Farley MM,
657 Holzbauer SM, Meek JI, Phipps EC, Wilson LE, Winston LG, Cohen JA, Limbago BM,
658 Fridkin SK, Gerding DN, McDonald LC. 2015. Burden of *Clostridium difficile* infection
659 in the United States. N Engl J Med 372:825-34.
660 3. Deakin LJ, Clare S, Fagan RP, Dawson LF, Pickard DJ, West MR, Wren BW,
661 Fairweather NF, Dougan G, Lawley TD. 2012. The C*lostridium difficile spo0A* gene is a
662 persistence and transmission factor. Infect Immun 80:2704-11.
663 4. Dembek M, Willing SE, Hong HA, Hosseini S, Salgado PS, Cutting SM. 2017. Inducible
664 Expression of spo0A as a Universal Tool for Studying Sporulation in *Clostridium*
665 *difficile*. Front Microbiol 8:1793.
666 5. Paredes-Sabja D, Shen A, Sorg JA. 2014. *Clostridium difficile* spore biology: sporulation,
667 germination, and spore structural proteins. Trends Microbiol 22:406-16.
668 6. Chandrasekaran R, Lacy DB. 2017. The role of toxins in *Clostridium difficile* infection.
669 FEMS Microbiol Rev 41:723-750.
670 7. Jump RL, Pultz MJ, Donskey CJ. 2007. Vegetative *Clostridium difficile* survives in room
671 air on moist surfaces and in gastric contents with reduced acidity: a potential mechanism
672 to explain the association between proton pump inhibitors and *C. difficile*-associated
673 diarrhea? Antimicrob Agents Chemother 51:2883-7.
674 8. Koenigsknecht MJ, Theriot CM, Bergin IL, Schumacher CA, Schloss PD, Young VB.
675 2015. Dynamics and establishment of *Clostridium difficile* infection in the murine
676 gastrointestinal tract. Infect Immun 83:934-41.
677 9. Tan IS, Ramamurthi KS. 2014. Spore formation in *Bacillus subtilis*. Environ Microbiol
678 Rep 6:212-25.
679 10. Driks A, Eichenberger P. 2016. The Spore Coat. Microbiol Spectr 4.
680 11. Setlow P. 2014. Germination of spores of *Bacillus* species: what we know and do not
681 know. J Bacteriol 196:1297-305.
682 12. McKenney PT, Driks A, Eichenberger P. 2012. The *Bacillus subtilis* endospore:
683 assembly and functions of the multilayered coat. Nat Rev Microbiol
684 doi:10.1038/nrmicro2921.
685 13. Gill RL, Jr., Castaing JP, Hsin J, Tan IS, Wang X, Huang KC, Tian F, Ramamurthi KS.
686 2015. Structural basis for the geometry-driven localization of a small protein. Proc Natl
687 Acad Sci U S A 112:E1908-15.
688 14. Ramamurthi KS, Clapham KR, Losick R. 2006. Peptide anchoring spore coat assembly to
689 the outer forespore membrane in *Bacillus subtilis*. Mol Microbiol 62:1547-1557.
690 15. Ramamurthi KS, Losick R. 2008. ATP-driven self-assembly of a morphogenetic protein
691 in *Bacillus subtilis*. Mol Cell 31:406-14.
692 16. McKenney PT, Eichenberger P. 2012. Dynamics of spore coat morphogenesis in *Bacillus*
693 *subtilis*. Mol Microbiol 83:245-60.
694 17. Wang KH, Isidro AL, Domingues L, Eskandarian HA, McKenney PT, Drew K,
695 Grabowski P, Chua MH, Barry SN, Guan M, Bonneau R, Henriques AO, Eichenberger P.

2009. The coat morphogenetic protein SpoVID is necessary for spore encasement in *Bacillus subtilis*. Mol Microbiol 74:634-49.

18. Roels S, Driks A, Losick R. 1992. Characterization of *spoIVA*, a sporulation gene involved in coat morphogenesis in *Bacillus subtilis*. J Bacteriol 174:575-585.
19. Beall B, Driks A, Losick R, Moran CP, Jr. 1993. Cloning and characterization of a gene required for assembly of the *Bacillus subtilis* spore coat. J Bacteriol 175:1705-16.
20. Levin PA, Fan N, Ricca E, Driks A, Losick R, Cutting S. 1993. An unusually small gene required for sporulation by *Bacillus subtilis*. Mol Microbiol 9:761-71.
21. Tan IS, Weiss CA, Popham DL, Ramamurthi KS. 2015. A Quality-Control Mechanism Removes Unfit Cells from a Population of Sporulating Bacteria. Dev Cell 34:682-93.
22. Fernandes CG, Moran CP, Jr., Henriques AO. 2018. Autoregulation of SafA Assembly through Recruitment of a Protein Cross-Linking Enzyme. J Bacteriol 200.
23. Galperin MY, Mekhedov SL, Puigbo P, Smirnov S, Wolf YI, Rigden DJ. 2012. Genomic determinants of sporulation in Bacilli and Clostridia: towards the minimal set of sporulation-specific genes. Environ Microbiol 14:2870-2890.
24. Henriques AO, Moran CP, Jr. 2007. Structure, assembly, and function of the spore surface layers. Annu Rev Microbiol 61:555-88.
25. Putnam EE, Nock AM, Lawley TD, Shen A. 2013. SpoIVA and SipL are *Clostridium difficile* spore morphogenetic proteins. J Bacteriol 195:1214-25.
26. Ribis JW, Ravichandran P, Putnam EE, Pishdadian K, Shen A. 2017. The Conserved Spore Coat Protein SpoVM Is Largely Dispensable in *Clostridium difficile* Spore Formation. mSphere 2.
27. Ribis JW, Fimlaid KA, Shen A. 2018. Differential requirements for conserved peptidoglycan remodeling enzymes during *Clostridioides difficile* spore formation. Mol Microbiol 110:370-389.
28. Ng YK, Ehsaan M, Philip S, Collery MM, Janoir C, Collignon A, Cartman ST, Minton NP. 2013. Expanding the repertoire of gene tools for precise manipulation of the *Clostridium difficile* genome: allelic exchange using *pyrE* alleles. PLoS One 8:e56051.
29. Collery MM, Kuehne SA, McBride SM, Kelly ML, Monot M, Cockayne A, Dupuy B, Minton NP. 2016. What's a SNP between friends: The influence of single nucleotide polymorphisms on virulence and phenotypes of *Clostridium difficile* strain 630 and derivatives. Virulence doi:10.1080/21505594.2016.1237333:0.
30. Fimlaid KA, Jensen O, Donnelly ML, Siegrist MS, Shen A. 2015. Regulation of *Clostridium difficile* Spore Formation by the SpoIIQ and SpoIIIA Proteins. PLoS Genet 11:e1005562.
31. Fimlaid KA, Bond JP, Schutz KC, Putnam EE, Leung JM, Lawley TD, Shen A. 2013. Global Analysis of the Sporulation Pathway of *Clostridium difficile*. PLoS Genet 9:e1003660.
32. Pereira FC, Nunes F, Cruz F, Fernandes C, Isidro AL, Lousa D, Soares CM, Moran CP, Jr., Henriques AO, Serrano M. 2018. A LysM domain intervenes in sequential protein-protein and protein-peptidoglycan interactions important for spore coat assembly in *Bacillus subtilis*. J Bacteriol doi:10.1128/JB.00642-18.
33. Yutin N, Galperin MY. 2013. A genomic update on clostridial phylogeny: Gram-negative spore formers and other misplaced clostridia. Environ Microbiol 15:2631-2641.
34. Sasi Jyothsna TS, Tushar L, Sasikala C, Ramana CV. 2016. Paraclostridium benzoelyticum gen. nov., sp. nov., isolated from marine sediment and reclassification of

Clostridium bifermentans as *Paraclostridium bifermentans* comb. nov. Proposal of a new genus *Paeniclostridium* gen. nov. to accommodate *Clostridium sordellii* and *Clostridium ghonii*. Int J Syst Evol Microbiol 66:1268-1274.

35. Dworkin J. 2018. Detection of fungal and bacterial carbohydrates: Do the similar structures of chitin and peptidoglycan play a role in immune dysfunction? PLoS Pathog 14:e1007271.
36. Mesnage S, Dellarole M, Baxter NJ, Rouget JB, Dimitrov JD, Wang N, Fujimoto Y, Hounslow AM, Lacroix-Desmazes S, Fukase K, Foster SJ, Williamson MP. 2014. Molecular basis for bacterial peptidoglycan recognition by LysM domains. Nat Commun 5:4269.
37. Yang J, Yan R, Roy A, Xu D, Poisson J, Zhang Y. 2015. The I-TASSER Suite: protein structure and function prediction. Nat Methods 12:7-8.
38. Ozin A, Samford C, Henriques A, Moran C. 2001. SpoVID guides SafA to the spore coat in *Bacillus subtilis*. J Bacteriol 183:3041-3049.
39. Ozin AJ, Henriques AO, Yi H, Moran CP, Jr. 2000. Morphogenetic proteins SpoVID and SafA form a complex during assembly of the *Bacillus subtilis* spore coat. J Bacteriol 182:1828-33.
40. Castaing J-P, Nagy A, Anantharaman V, Aravind L, Ramamurthi K. 2013. ATP hydrolysis by a domain related to translation factor GTPases drives polymerization of a static bacterial morphogenetic protein. Proc Natl Acad Sci o 110:60.
41. Pogliano J, Osborne N, Sharp MD, Abanes-De Mello A, Perez A, Sun YL, Pogliano K. 1999. A vital stain for studying membrane dynamics in bacteria: a novel mechanism controlling septation during *Bacillus subtilis* sporulation. Mol Microbiol 31:1149-59.
42. Sorg JA, Dineen SS. 2009. Laboratory maintenance of *Clostridium difficile*. Curr Protoc Microbiol Chapter 9:Unit 9A 1.
43. Karasawa T, Ikoma S, Yamakawa K, Nakamura S. 1995. A defined growth medium for *Clostridium difficile*. Microbiology 141 (Pt 2):371-5.
44. Donnelly ML, Li W, Li YQ, Hinkel L, Setlow P, Shen A. 2017. A *Clostridium difficile*-Specific, Gel-Forming Protein Required for Optimal Spore Germination. mBio 8.
45. Shen A, Fimlaid KA, Pishdadian K. 2016. Inducing and Quantifying *Clostridium difficile* Spore Formation. Methods Mol Biol 1476:129-42.
46. Adams CM, Eckenroth BE, Putnam EE, Doublie S, Shen A. 2013. Structural and functional analysis of the CspB protease required for *Clostridium* spore germination. PLoS Pathog 9:e1003165.
47. Kevorkian Y, Shirley DJ, Shen A. 2015. Regulation of *Clostridium difficile* spore germination by the CspA pseudoprotease domain. Biochimie doi:10.1016/j.biochi.2015.07.023.
48. Ransom EM, Ellermeier CD, Weiss DS. 2015. Use of mCherry Red fluorescent protein for studies of protein localization and gene expression in *Clostridium difficile*. Appl Environ Microbiol 81:1652-60.

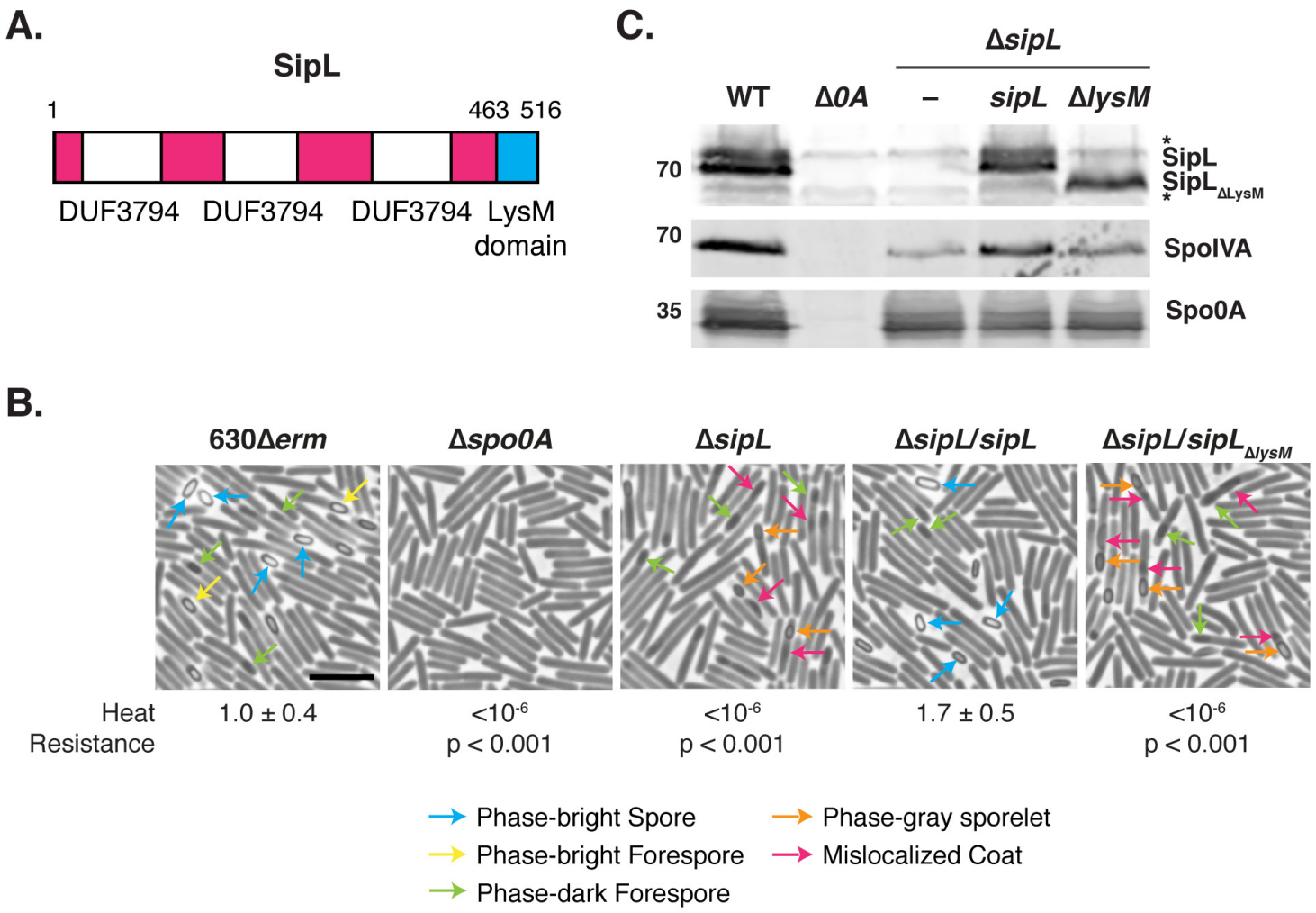

Figure 1. The LysM domain of *C. difficile* is essential for spore formation. (A) Schematic of *C. difficile* SipL domain structure. SipL contains three domains of unknown function (DUF3794) and a C-terminal LysM domain. (B) Phase-contrast microscopy analyses of the indicated *C. difficile* strains ~20 hrs after sporulation induction. Δ*sipL* was complemented with either the wild-type allele or one encoding a deletion of the LysM domain (Δ*sipL*/*sipL*$_{\Delta lysM}$). Arrows mark examples of sporulating cells at different stages of maturation: blue arrows highlight phase-bright free spores; yellow arrows mark mature phase-bright forespores, which are formed following cortex formation (22, 24); green arrows highlight immature phase-dark forespores; orange arrows highlight phase-gray sporelets, which produce a phase-dark ring surrounding the forespore but do not become phase-bright; and pink arrows demarcate regions suspected to be mislocalized coat based on previous studies (26, 30). Heat resistance efficiencies were determined from 20-24 hr sporulating cultures and represent the mean and standard deviation for a given strain relative to wild type based on a minimum of three independent biological replicates. Statistical significance relative to wild type was determined using a one-way ANOVA and Tukey's test. Scale bar represents 5 μm. The limit of detection of the assay is 10^{-6}. (C) Western blot analyses of SipL, SpoIVA, and Spo0A. SipL was detected using an antibody raised against SipL lacking its LysM domain (i.e. SipL$_{\Delta LysM}$). Asterisks indicate non-specific bands detected by the SipL$_{\Delta LysM}$ antibody. SpoIVA levels were analyzed because of the prior finding that SpoIVA levels are reduced in the absence of SipL (25). Modest decreases in SipL levels were observed in the Δ*sipL* and Δ*sipL*/*sipL*$_{\Delta lysM}$ strains. Spo0A was used as a proxy for measuring sporulation induction (4, 25). The western blots shown are representative of the results of three independent biological replicates.

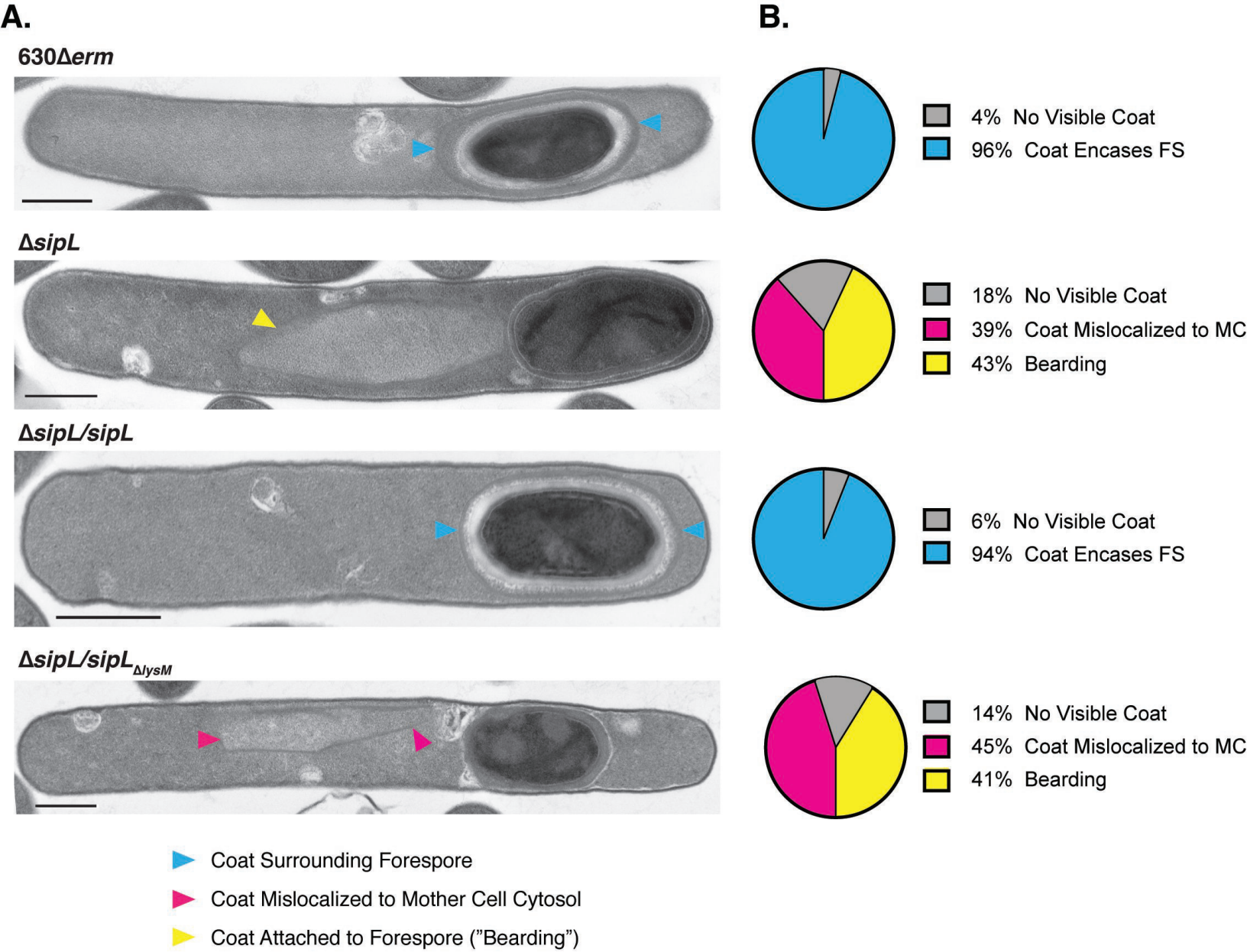

Figure 2. Loss of SipL's LysM domain results in coat mislocalization defects. (A) Transmission electron microscopy (TEM) analyses of wild-type 630Δ*erm*, Δ*sipL*, and Δ*sipL* complemented with either wild-type *sipL* or *sipL* encoding a LysM deletion ($sipL_{\Delta lysM}$) after 23 hrs of sporulation induction. Scale bars represent 500 nm. Blue arrows mark properly localized coat, i.e. surrounding the entire forespore (FS), whereas pink arrows mark coat that has completely detached from the forespore and is found exclusively in the mother cell (MC) cytosol. Yellow arrows mark cells where coat appears to be detaching from the forespore but remains partially associated, also known as "bearding" (26). The percentages shown are based on analyses of at least 50 cells for each strain with visible signs of sporulation from a single biological replicate.

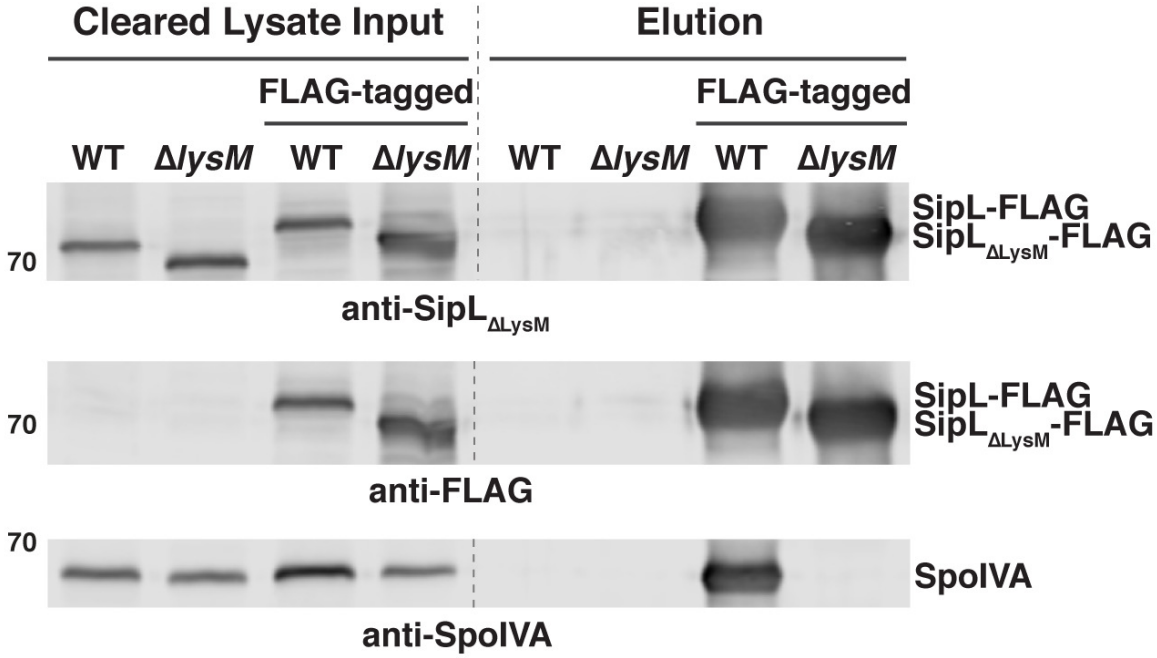

Figure 3. The LysM domain is required for SipL to bind SpoIVA in sporulating *C. difficile* cultures. FLAG-tagged SipL was immunoprecipitated from cleared lysates prepared from the indicated *C. difficile* Δ*sipL* complementation cultures ("Input" fraction) using anti-FLAG magnetic beads. Proteins bound to the beads after several washes were eluted using FLAG peptide ("Elution" fraction). "WT" indicates that Δ*sipL* was complemented with the wild-type *sipL* allele, whereas "Δ*lysM*" indicates that Δ*sipL* was complemented with a *sipL*$_{ΔlysM}$ construct. "FLAG-tagged" indicates that the complementation constructs encoded a C-terminal FLAG tag consisting of three successive FLAG tags, which resulted in the SipL-FLAG fusions exhibiting a higher mobility during SDS-PAGE. The untagged *sipL* complementation strains served as negative controls to ensure that untagged SipL and SpoIVA were not non-specifically pulled-down by the anti-FLAG beads. Sporulation was induced for 24 hrs before lysates were prepared. The immunoprecipitations shown are representative of three independent biological replicates.

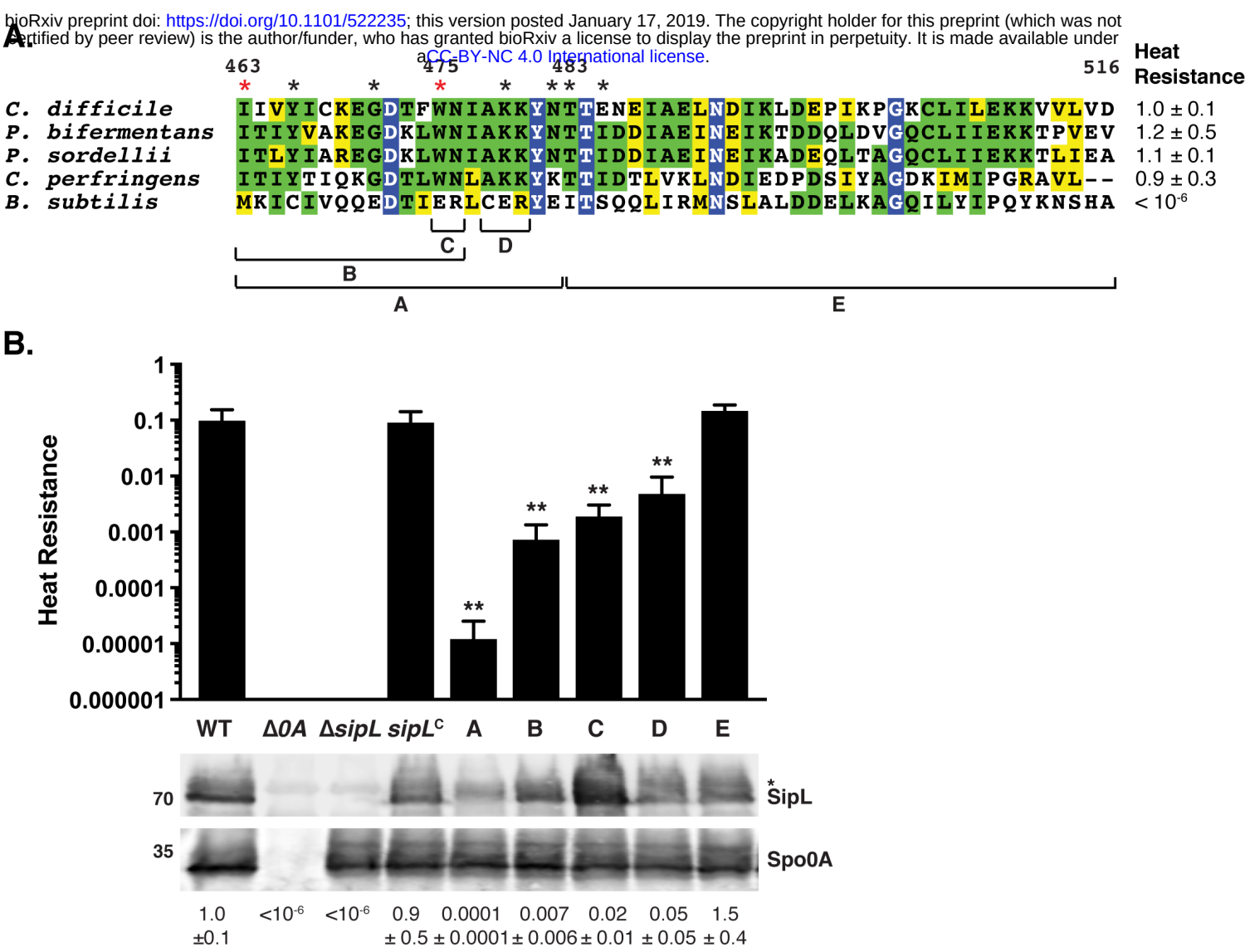

Figure 4. Chimeric analyses identify a small region of the LysM domain important for SipL function. (A) Alignment of LysM domains from SipL homologs from *C. difficile* (CAJ70473), *P. bifermentans* (EQK49575), *P. sordellii* (EPZ54296), and *C. perfringens* (YP_696893), as well as the LysM domain from *B. subtilis* SpoVID (NP_390689). Blue boxes with white text indicate residues that are completely conserved; green boxes indicate residues that are conserved in some of the homologs; and yellow boxes mark residues that are similar between the homologs. The brackets and letters below the alignment indicate the regions swapped between the *C. difficile* SipL and *B. subtilis* SpoVID LysM domains. The red asterisks highlight residues whose mutations impaired functional spore formation, while black asterisks indicate residues whose mutation to the residue in the *B. subtilis* SpoVID LysM domain did not reduce SipL function, i.e. spore formation (**Fig. S3**). (B) Graphical representation of the heat resistance assay results and western blot analyses of SipL in the chimeric constructs in (A) using an antibody raised against SipL lacking the LysM domain. *sipL*^{C} refers to the Δ*sipL*/*sipL* wild-type complementation strain. Asterisk marks a non-specific band detected by the anti-SipL$_{\Delta LysM}$ antibody. Spo0A was used as a proxy for measuring sporulation induction (4, 25). The western blots shown are representative of the results of three independent biological replicates. The heat resistance efficiencies for all chimeric swaps were determined from 20-24 hr sporulating cultures and represent the mean and standard deviation for a given strain relative to wild type based on a minimum of three independent biological replicates. Statistical significance relative to wild type was determined using a one-way ANOVA and Tukey's test. ** $p < 0.01$.

his same study showed that

A.

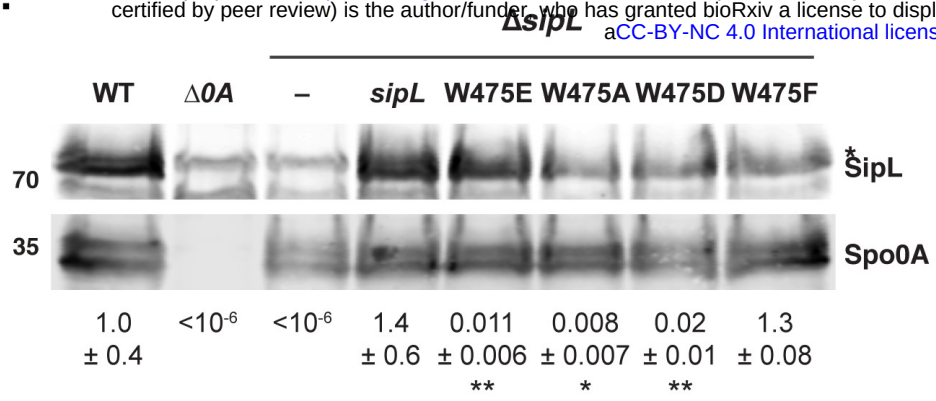

B.

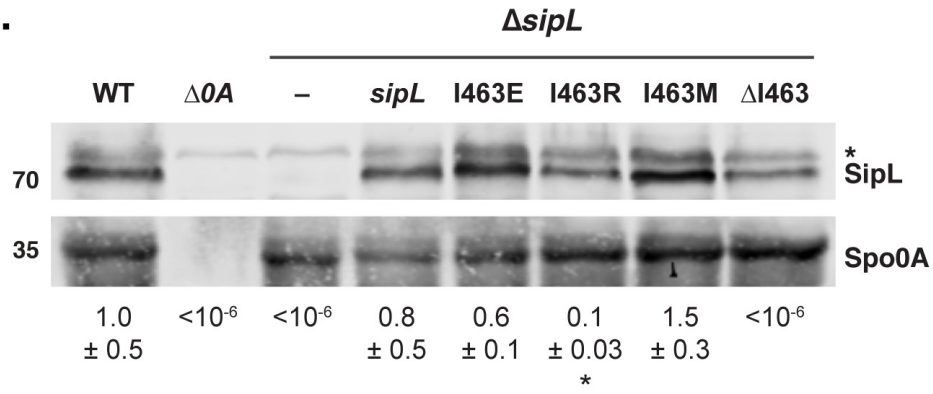

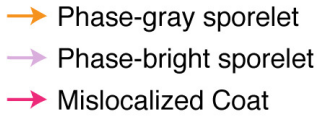

C.

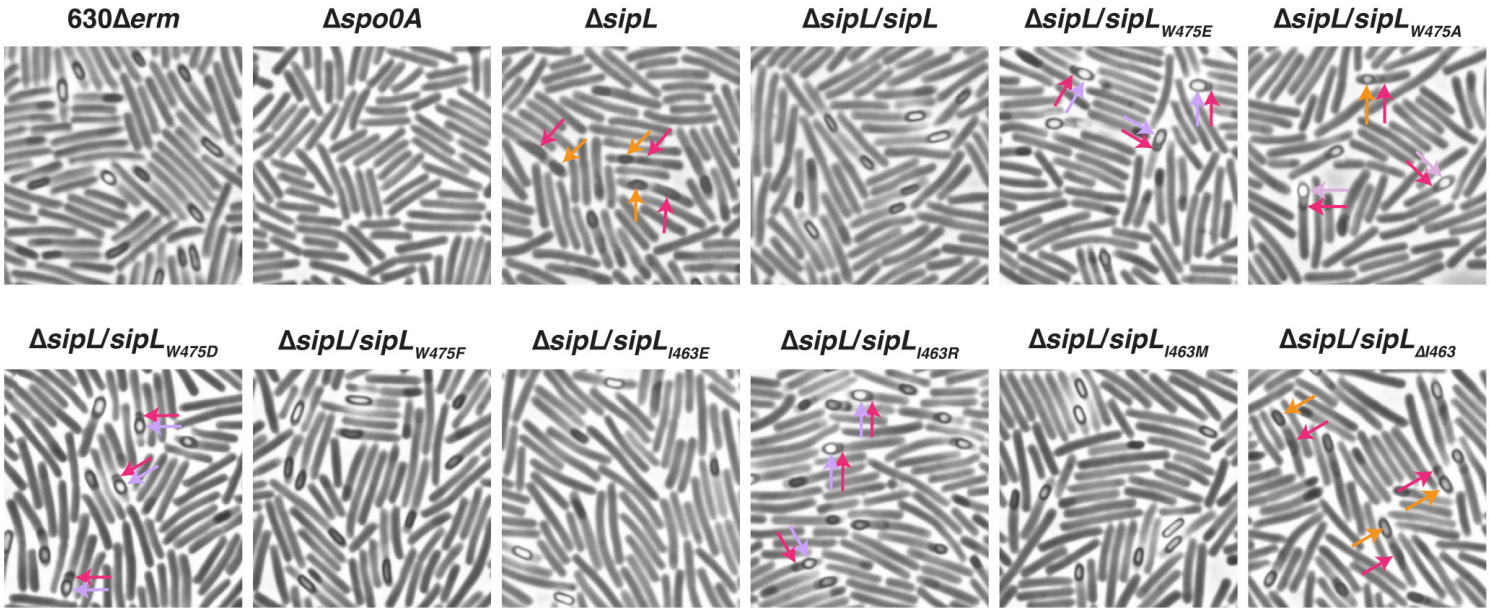

D.

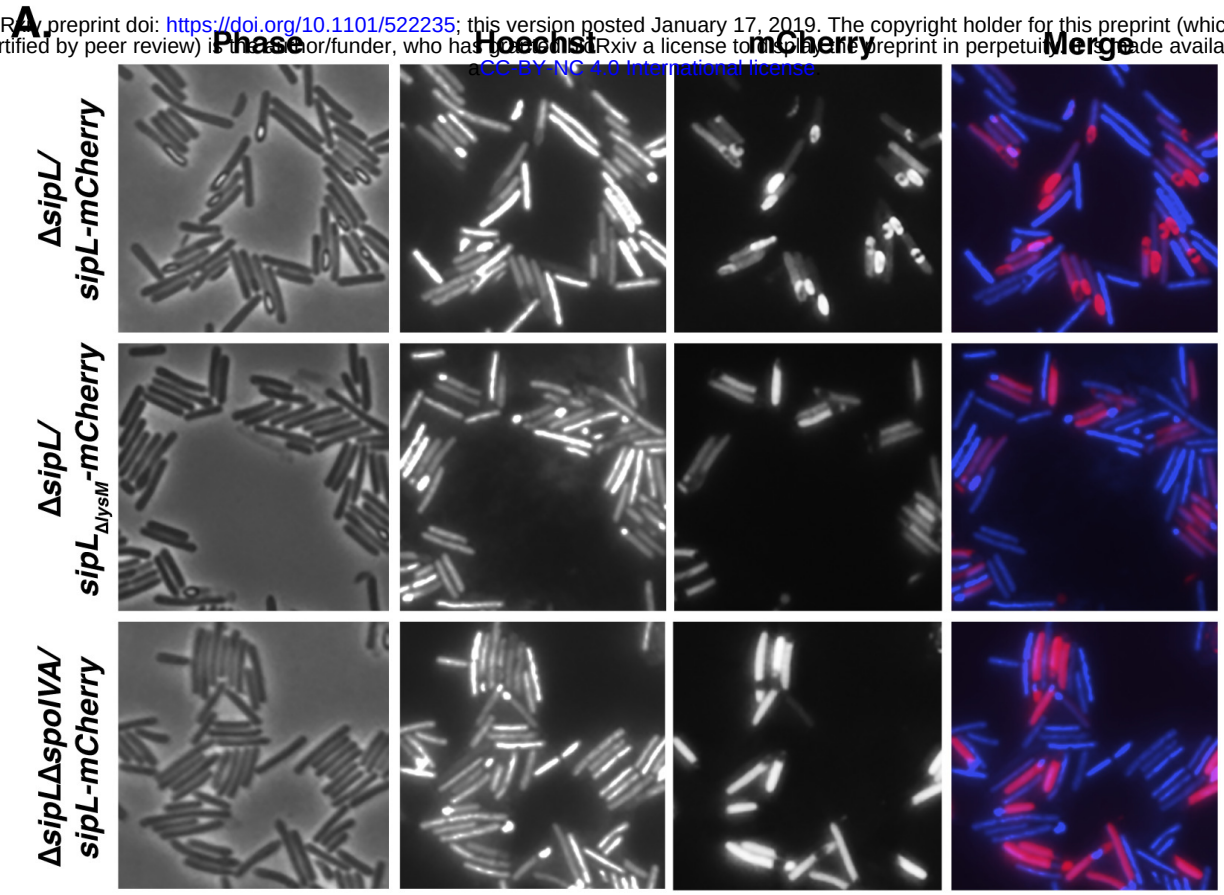

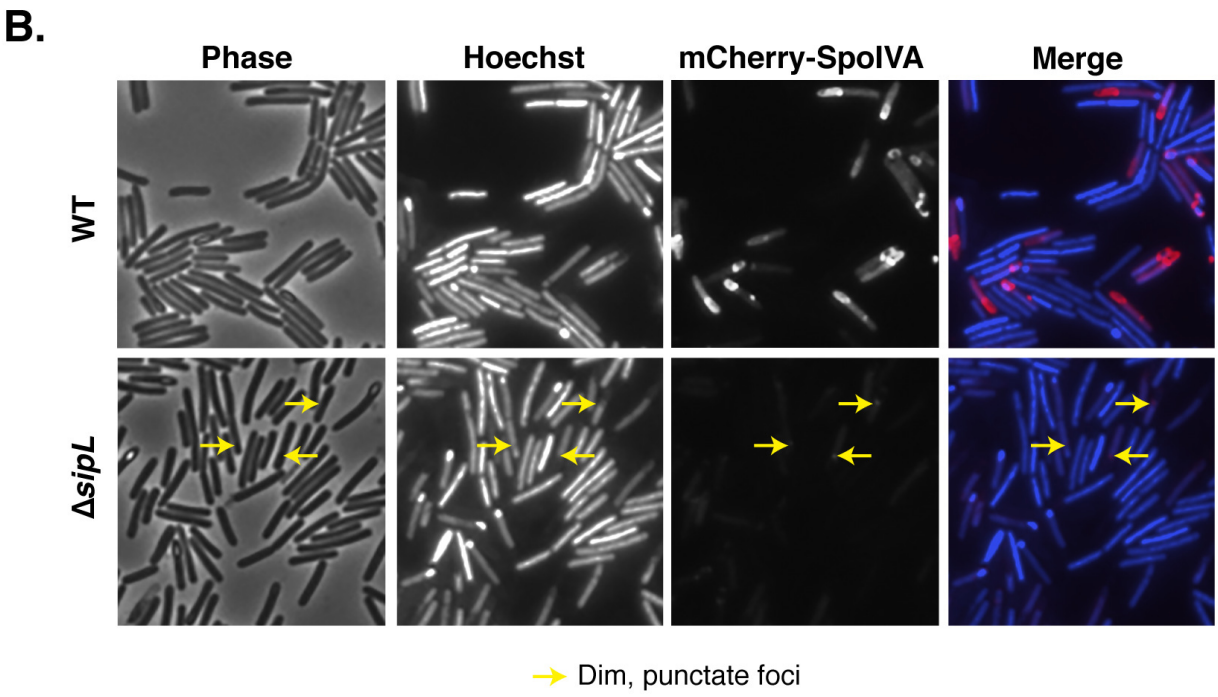

→ Dim, punctate foci

Figure 6. SipL binding to SpoIVA is required to localize SipL to the forespore, while SpoIVA encasement of the forespore depends on SipL. (A) Fluorescence microscopy analyses of either Δ*sipL* or Δ*sipL*Δ*spoIVA* complemented with constructs encoding either SipL-mCherry or SipL$_{ΔLysM}$-mCherry after 20-23 hrs post-sporulation induction. (B) mCherry-SpoIVA localization in either the wild-type or Δ*sipL* strain backgrounds. A wild-type copy of *spoIVA* was present in both strains because the fusion protein does not efficiently encase the forespore unless a wild-type copy of *spoIVA* is present (26). Cells were visualized using phase-contrast (phase) microscopy, and the nucleoid was visualized using Hoechst staining (41). The Hoechst-stained nucleoid is shown in blue, and mCherry fluorescence is shown in red. Engulfment completion excludes Hoechst from staining the forespore (41). The merge of Hoechst and mCherry is also shown. Yellow arrows mark single, dim foci of mCherry-SpoIVA observed in the Δ*sipL* strain background. The images shown are representative of three independent biological replicates.